Magnetic Resonance Imaging Evidence For Widespread Orbital Dysinnervation in Congenital Fibrosis of Extraocular Muscles Due to Mutations in *KIF21A*

Joseph L. Demer,[1,2,3] *Robert A. Clark,*[1] *and Elizabeth C. Engle*[4,5,6]

Purpose. High-resolution orbital magnetic resonance imaging (MRI) was used to investigate the structural basis of ocular motility abnormalities in humans with congenital fibrosis of the extraocular muscles type 1 (CFEOM1) due to missense mutations in the developmental kinesin *KIF21A*.

Methods. Clinical ophthalmic and motility findings in 19 volunteers from six unrelated CFEOM1 pedigrees harboring four of the six reported *KIF21A* mutations and 23 normal control subjects were correlated with MRI studies demonstrating extraocular muscle (EOM) size, location, contractility, and innervation.

Results. Subjects with CFEOM1 had severe bilateral blepharoptosis, limited supraduction, and variable ophthalmoplegia. In affected subjects, MRI demonstrated atrophy of the levator palpebrae superioris and superior rectus EOMs and small or absent orbital motor nerves. The oculomotor nerve was most severely hypoplastic, but the abducens was also affected. EOMs exhibited variable atrophy and an abnormally bright T1 signal. Subjects with the R954W and R954Q substitutions frequently exhibited A-pattern strabismus, with misinnervation of the lateral rectus muscle by an oculomotor nerve branch. Rectus pulley locations were generally normal. Subjects with CFEOM1 exhibited subclinical but highly significant reduction from normal in mean optic nerve size ($P < 0.001$). Comparing clinical and MRI phenotypes did not reveal distinguishing features among *KIF21A* mutations.

Conclusions. Orbital imaging in CFEOM1 due to various amino acid substitutions in the kinesin *KIF21A* demonstrates consistent abnormalities of motor and sensory innervation in the orbit. These findings suggest that neuronal disease is primary in CFEOM1, with myopathy arising secondary to abnormal innervation and minimal rectus pulley abnormality secondary to reduced EOM forces. (*Invest Ophthalmol Vis Sci.* 2005;46:530–539) DOI:10.1167/iovs.04-1125

From the Jules Stein Eye Institute, Departments of [1]Ophthalmology, [2]Neurology, and [3]Bioengineering, and Neuroscience Interdepartmental Programs, University of California, Los Angeles; the Departments of [4]Medicine (Genetics and Genomics) and [5]Neurology, Children's Hospital, Boston, Massachusetts; and [6]Department of Neurology, Harvard Medical School, Boston, Massachusetts.

Supported by National Eye Institute Grants EY13583, EY08313, and EY00331. JLD received an unrestricted award from Research to Prevent Blindness and is the Grace and Walter Lance Professor of Ophthalmology.

Submitted for publication September 21, 2004; revised November 3, 2004; accepted November 14, 2004.

Disclosure: **J.L. Demer**, None; **R.A. Clark**, None; **E.C. Engle**, None

The publication costs of this article were defrayed in part by page charge payment. This article must therefore be marked "*advertisement*" in accordance with 18 U.S.C. §1734 solely to indicate this fact.

Corresponding author: Joseph L. Demer, Jules Stein Eye Institute, 100 Stein Plaza, UCLA, Los Angeles, CA 90095-7002; jld@ucla.edu.

Congenital fibrosis of the extraocular muscles (CFEOM) is a typically nonprogressive disorder of ocular motility with accompanying blepharoptosis. Three distinct phenotypes, CFEOM1 to -3, are recognized. The classic form of CFEOM, CFEOM1 (Mendelian Inheritance in Man [MIM] 135700; http://www.ncbi.nlm.nih.gov/Omim/, provided in the public domain by the National Center for Biotechnology Information, Bethesda, MD) is typified by congenital bilateral blepharoptosis and ophthalmoplegia, with the eyes partially or completely fixed in infraduction.[1] Horizontal strabismus may coexist. CFEOM1 is autosomal dominant and maps to chromosome 12.[2,3] Recently, CFEOM1 has been shown to result from a small number of recurrent heterozygous missense mutations of the kinesin motor protein encoded by *KIF21A*.[4]

Forced duction testing in individuals with CFEOM1 demonstrates marked restriction of passive elevation of the globes, consistent with surgical observations of increased extraocular muscle (EOM) stiffness. Older pathologic reports of specimens of resected EOMs in CFEOM suggested that they were replaced entirely[5–8] or in part[9,10] by fibrous tissue. The classic suggestion that CFEOM is due to primary myopathy, however, has been challenged by the autopsy findings in an affected member of a pedigree later shown to harbor the common *KIF21A* mutation.[1–4] There was absence of the superior division of the oculomotor nerve (n. III) and its corresponding α motor neurons, as well as marked reduction in the number of axons in the proximal n. III.[1] Absence of axonal degeneration suggests that the missing nerve fibers were never present. The superior rectus (SR) and levator palpebrae superioris (LPS) EOMs, normally innervated by the superior division of n. III, could not be identified grossly at autopsy and were represented microscopically by a single small structure containing fat, fibrous tissue, and sparse myofibers. Although the remaining EOMs were innervated and exhibited no abnormal fibrosis, internal nuclei, and mitochondrial clumping were observed in EOMs innervated by the inferior division of n. III as well as the trochlear (n. IV) and abducens (n. VI) nerves.[1] Engle et al.[1] therefore suggested that CFEOM1 is a primary disorder of EOM lower motor neuron development, leading to hypoplasia or atrophy of the EOMs they innervate and to secondary contracture of their antagonists. Older reports of "fibrosis" in EOM tendons are thought to be artifacts of inadvertent biopsy of distal EOM tendons.[1]

The neuropathic hypothesis for CFEOM1 is further supported by both clinical and genetic findings. The frequent occurrence of synergistic eye movements and the Marcus Gunn jaw winking phenomenon in individuals with CFEOM1 secondary to *KIF21A* mutations[1,3,4,11–13] is suggestive of misrouting of motor axons. The mutated gene *KIF21A*, encodes a motor protein expressed in early development[4] and is involved in anterograde axonal transport.[14] In its mutated state, the axonal transport of a cargo critical to the development of ocular motor nerves may be disrupted, resulting in a primary neuropathy. This neuropathic hypothesis however, can still be challenged. Kinesins have been shown to be expressed in skeletal muscle[15] and expression and function of

KIF21A within EOM that is critical to the development of these muscles has not been excluded. It also remains possible that the neuropathologic findings in the isolated autopsy case do not generalize to other affected individuals.

Technical improvements in magnetic resonance imaging (MRI) now afford the opportunity for detailed study of the functional anatomy of EOMs and nerves in the orbits of living subjects,[16] and cranial nerves can be imaged against the surrounding cerebrospinal fluid (CSF) as they exit the brain stem.[17] The present study was performed to characterize the structure and function of EOMs, and the structure of orbital innervation, in a large number of subjects with CFEOM1 resulting from four of the six published mutations in *KIF21A*. The findings define a reproducible endophenotype, demonstrate that the specific *KIF21A* mutations underlying CFEOM1 cannot be predicted based on phenotype, and strongly support the neuropathic hypothesis of CFEOM, extending the recognized involvement beyond motor nerves to the optic nerve (ON) as well.

METHODS

High-resolution MRI images were collected from volunteers who gave written informed consent to a protocol conforming to the Declaration of Helsinki and approved by the Institutional Review Boards of the University of California, Los Angeles, and The Children's Hospital Boston. Paid normal control subjects were recruited by advertising, and subjects with CFEOM1 due to *KIF21A* mutations were recruited through an ongoing genetic study of CFEOM.[4] All normal and affected subjects underwent complete ophthalmic examination of corrected visual acuity, ocular motility, eyelid structure and function, binocular alignment, anterior segment anatomy, and ophthalmoscopy. Ophthalmic histories were obtained from subjects with CFEOM1, with corroboration of previous ocular surgeries from operative records where possible. In addition to the preceding examinations, subjects with CFEOM1 also underwent measurement of palpebral fissure height and levator function, with video recording of ocular versions, eyelid motility, and an attempt to elicit Bell's phenomenon of involuntary supraduction on attempted eyelid closure. In many affected subjects, forced duction testing was performed under topical anesthesia with topical proparacaine 0.5% and use of a toothed forceps to manipulate the eye passively.

Imaging was performed with a 1.5-Tesla scanner (Signa; General Electric, Milwaukee, WI). Orbital imaging was performed with an array of surface coils embedded in a transparent face mask (Medical Advances, Milwaukee, WI) and fixation targets, to avoid eye motion artifacts.[18,19] The head was stabilized in the supine position by tightly fastening the surface coil mask to the face with headbands and fixing the mask to the scanner gantry with foam cushions and tape. These measures avoided head rotation during scanning. An adjustable array of illuminated fixation targets was secured in front of each orbit, with the center target in subjective central position for each eye and, in selected cases, in secondary and tertiary gaze positions. Imaging at and posterior to the orbital apex in some subjects was performed with the standard head coil. When surface coils were used, images of 2-mm thickness in a matrix of 256 × 256 were obtained over a field of view of 6 to 8 cm for a resolution in-plane of 234 to 312 μm, respectively. Axial scout images were obtained, as well as quasicoronal images perpendicular to the long axis of the orbit, and quasisagittal images parallel to the long axis of the orbit. Imaging of the deeper portions of motor nerves innervating the EOMs was performed in 1-mm thickness image planes, by using the heavily T2-weighted FIESTA sequence, which provides good contrast of the cranial nerves against the surrounding cerebrospinal fluid.[17] In-plane resolution was 195 μm over a 10-cm field of view (matrix 512 × 512) with 10 excitations.

Digital MRI images were transferred to computers (Macintosh; Apple Computer, Cupertino, CA), converted into 8-bit tagged image file format (TIFF), and quantified with NIH Image (Wayne Rasband, National Institutes of Health; available by ftp from zippy.nimh.nih.gov or on floppy disc from NTIS, Springfield, VA, part number PB95-500195GEI).

In coronal planes, the location of each rectus EOM was described by a single point in each image plane by using the "area centroid" function of the NIH Image program according to a method previously described in detail.[20] The area centroid of a cross section is equivalent to the center of gravity of a shape of uniform density and thickness. Next, approximating the globe as spherical, its 3-D center was determined to subpixel resolution in scanner coordinates by using curve-fitting to cross-sectional images of the globe, as previously described.[19] Rectus EOM positions were then translated to place the 3-D coordinate origin at the computed center of the globe. After data were transformed, the scanner coordinates were scaled to millimeters. Coronal plane rectus pulley locations were determined from the EOM centroid coordinates at the anteroposterior positions determined in central gaze for each of the four rectus EOMs.[19] Inferior oblique (IO) muscles were analyzed in outlined cross sections in quasisagittal images, using an analogous procedure previously described in detail.[21]

RESULTS

Subjects

Nineteen volunteers with CFEOM1 due to heterozygous missense mutations of *KIF21A* were ascertained from six unrelated kindreds. When possible, these volunteers were recruited to permit the comparison of images from different members of the same pedigree, different pedigrees with the identical mutation, and pedigrees with different mutations. Fourteen volunteers from three pedigrees harbored the most common 2860C→T mutation that results in an R954W amino acid substitution; two volunteers from one pedigree harbored the second most common mutation, 2861G→A, which alters the same amino acid (R954Q); two volunteers from one pedigree harbored the M356T substitution (1067T→C); and one volunteer harbored the M947R substitution (2840T→G). General characteristics of these subjects are summarized in Table 1, and include data on 10 males and 9 females with an average age of 29.8 ± 22.3 years (mean ± SD, range, 2–76). Each of the pedigree structures and molecular genetic confirmation of the mutations are reported elsewhere.[4] Interpretable MRI of the orbits was obtained in 14 affected subjects and of the skull base in two affected subjects; three children were too young to cooperate with scanning, and two subjects had permanent metallic dental appliances that produced imaging artifacts unacceptable for quantitative interpretation. The mean age of affected subjects who underwent MRI was 37.1 ± 21.6 years (range, 10–76).

A total of 23 normal volunteers, 12 male and 11 female, underwent orbital MRI scanning. Six of these normal volunteers underwent MRI of the cranial nerves in the skull base. Control subjects were of average age 33 ± 14 years (mean ± SD, range, 19–69). Because the full group of control subjects had an average age younger than that of the subjects with CFEOM, an age- and gender-matched subgroup of 11 control subjects with average age of 39 ± 19 years was selected for some analyses. All control subjects had normal ocular and lid motility, and visual acuity in each eye correctable to 0 logarithm of the minimum angle resolvable in arcmin [logMAR] (20/20) or better.

Clinical Findings in CFEOM1

Because mean corrected visual acuity was identical in the left and right eyes of affected subjects (Table 1), acuity data were pooled for the two eyes. Mean corrected visual acuity over these 36 eyes was 0.31 ± 0.05 logMAR (mean ± SEM; range, −0.1–1.6). Although mean acuity was thus equivalent to

TABLE 1. Characteristics of Subjects with CFEOM1

Subject	Pedigree	Amino Acid Substitution	Age (y)	Sex	Corrected Visual Acuity		Horizontal Alignment	ECO	MRI
					Right (logMAR)	Left (logMAR)			
1	A	R954W	53	M	0.3	0.7	XT	Yes	Yes
2	A	R954W	11	M	0.3	0.3	XT	Yes	No
3	A	R954W	13	F	0.2	0.2	XT	Yes	No
4	A	R954W	37	F	0.3	0.7	A-ET	No	Yes
5	AA	R954W	10	M	−0.1	−0.1	A-XT	No	Yes
6	AA	R954W	13	M	0.0	0.0	A-XT	No	No
7	AA	R954W	17	F	0.05	0.25	A-XT	No	Yes
8	AA	R954W	18	M	0.3	0.3	XT	Yes	Yes
9	AA	R954W	11	F	0.2	0.2	A-XT	No	Yes
10	AA	R954W	76	F	0.3	0.3	XT	Yes	Yes
11	AA	R954W	52	M	1.6	0.05	XT	Yes	Yes
12	AA	R954W	57	M	0.2	0.4	Orthotropic	Yes	Yes
13	AA	R954W	67	M	0.2	0.48	XT	Yes	Yes
14	GF	R954W	28	M	0.4	0.3	XT	Yes	Yes
15	L	R954Q	35	F	0.2	0.5	A-XT	No	Yes
16	L	R954Q	2	F	—	—	A-XT	No	No
17	AV	M356T	43	F	0.2	0.3	XT	No	Yes
18	AV	M356T	8	M	0.2	0.2	ET	No	No
19	CA	M947R	15	F	0.8	0.55	ET	Yes	Yes
Mean			30		0.31	0.31			
SEM			5		0.09	0.05			

XT, exotropia; A-XT, A pattern exotropia; A-ET, A pattern esotropia; ECO, essentially complete ophthalmoplegia. All subjects had bilateral blepharoptosis and limited supraduction. Quantitative acuity could not be obtained in pre-literate Subject 16.

20/40, eight subjects had amblyopia, with interocular difference ranging from 0.2 to 1.55 logMAR (2–16 lines). All subjects with CFEOM who were old enough to be tested had normal visual fields in both eyes by confrontation screening.

As tested in a dark room, subjects with CFEOM had symmetrical pupils with a mean diameter of 4.2 ± 0.2 mm, significantly smaller than in the normal subjects (5.6 ± 0.4 mm; $P < 0.05$, one-tailed *t*-test). All subjects with CFEOM had symmetrical pupillary reactions to a bright, handheld light, without afferent pupillary defect or light-near dissociation, although subjects 1, 2, 9, 10, 11, 12, 14, and 19 had light reactivity noted as only slight. Pupillary reactions to near were not examined in all subjects with CFEOM, because presbyopic subjects lacking convergence and with large-angle exotropia at near were not expected to be able to make an interpretable near effort. However, six subjects with CFEOM exhibited normal meiosis during near viewing.

All 19 subjects with CFEOM had blepharoptosis with profoundly reduced to absent function of the levator palpebrae superioris (LPS) muscles bilaterally. Fifteen subjects had undergone between 1 and 4 surgeries each for ptosis correction, usually consisting of suspension of the upper eyelids from the frontalis muscles, so that the average number of ptosis surgeries undergone by all subjects with CFEOM was 1.2. Because this ptosis surgery interferes with complete eyelid closure, eight older patients with CFEOM exhibited exposure keratopathy, ranging from superficial punctate epithelial lesions to deep stromal scarring.

All but one subject with CFEOM1 had undergone between 1 and 7 operations for correction of strabismus, averaging 1.9 operations per subject. All subjects exhibited limitation of supraduction, with an asymmetry leading to gross vertical misalignment in two subjects. The precision of measurement of vertical binocular alignment was limited by the inability of most subjects to make the vertical eye movements required for prism and cover testing. Because most subjects had undergone surgery on the inferior rectus (IR) muscles and because this surgery would have influenced vertical alignment, quantitative measurements of vertical binocular alignment are not reported herein. All but five affected subjects either currently exhibited, or had reliable information indicating, the presence of exotropia in central gaze at least in early life (Table 1).

Ten subjects with CFEOM1 had bilateral generalized and essentially complete ophthalmoplegia (ECO). Forced-duction testing, performed in seven of these subjects under topical anesthesia, showed marked restriction to passive ocular rotation in all directions. In some subjects, however, there was the presence of low-amplitude abducting or infraducting movements with effort, or fine downbeat or torsional nystagmus best observed under magnification. Synergistic divergence was occasionally observed on attempted lateral gaze in subjects with ECO.

The remaining nine subjects with CFEOM1 were able to achieve at least some ocular ductions of grossly normal magnitude, and the seven of these with amino acid substitutions at position 954 (R954W and R954Q) had an incomitant pattern of orthotropia or esotropia in attempted upward gaze, and marked exotropia in attempted downward gaze, evocative of the letter A or λ. In several of these subjects, the λ pattern was highly suggestive of aberrant innervation of the lateral rectus (LR) muscle during infraduction, and LR inhibition during attempted supraduction (Fig. 1). Forced duction testing was performed in only one subject with A pattern and indicated generalized restriction to passive ocular rotation. Subject 9 with a λ pattern exhibited bilateral globe retraction with attempted upward gaze, and subject 4 had retraction on attempted abduction. The two subjects with the M356T amino acid substitution were able to make significant ocular rotations, but did not exhibit the A or λ pattern. In view of the small number of subjects with the M356T substitution, it is unclear whether the absence of this strabismus pattern is significant.

The ophthalmoscopic appearance of the ON head was normal in all subjects with CFEOM, with the exception of subject 4, who bilaterally exhibited the double-ring sign of a bare scleral annulus surrounding a central hypoplastic ON, and subject 18, who exhibited an apparently normal sized ON but

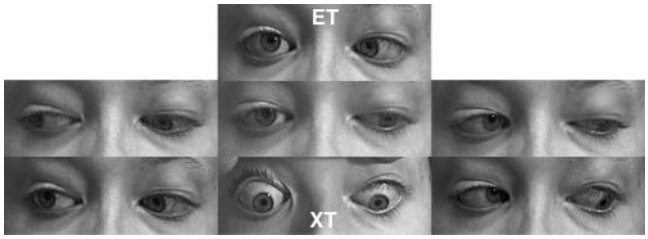

FIGURE 1. The A pattern in subject 7. Photographs show esotropia (ET) in attempted upward gaze and exotropia (XT) in central and downward gaze. There was marked limitation of the range of vertical gaze and hypotropia of the left eye. The upper eyelid configuration was created at surgery for blepharoptosis. The subject had also undergone strabismus surgery.

had a chorioretinal defect adjacent the superior margin of the optic disc.

Orbital Imaging Findings in CFEOM1

Extraocular Muscles. Despite prior strabismus surgery in many cases, orbital MRI was considered to provide a reasonable reflection of the sizes and positions of the rectus EOM bellies, since surgery is largely confined to the region of the insertional tendons. All subjects with CFEOM1 showed profound hypoplasia of the SR and LPS muscles, as illustrated in subject 7 in the coronal plane in Figure 2 and in the quasisagittal plane in Figure 3. It was often possible to detect the presence of these EOMs only in the quasisagittal MRI plane that had optimal resolution along the EOM paths, as the residual EOMs were markedly attenuated.

We computed rectus EOM volumes for subjects with CFEOM1, beginning with quantitative analysis of the largest and most homogeneous CFEOM1 subject group with the R954W amino acid substitution. These volumes included a total of contiguous six image planes beginning with the image plane that included the globe–ON junction and extending five image planes posteriorly. The volume computations thus did not include the region of the orbital apex, which was generally deep in relation to the field of imaging. Statistical analysis was performed in subjects with the R954W substitution, where a meaningful sample size was available (Table 2). The reduction from normal in SR volume computed from quasicoronal plane MRI ranged from 28% to 81% and averaged approximately 60% over all 11 of these subjects ($P < 0.000001$; Table 2). The medial rectus (MR) showed a 33% reduction in size from normal ($P < 0.000001$). There were smaller, insignificant volume reductions in the IR and LR muscles averaging 13% and 14%, respectively. At least some of these small IR and LR reductions may have resulted from prior surgeries to weaken these EOMs (such as the tenotomy that thinned the anterior portion of the IR in subject 7; Fig. 4), causing segmental shift of the volume of the contracted IR to the orbital apex outside the field of imaging). Comparing the data from pedigrees A and AA using *t*-tests for each of the rectus EOMs, we detected no significant interfamilial differences ($P \geq 0.15$). Recognizing the availability of only one representative of each pedigree having the remaining substitutions, we cautiously compared the data of pedigree AA with those obtained from subject 14 with the R954W substitution and subjects 15, 17, and 19 with the rarer KIF21A substitutions—R954Q, M356T, and M947R—respectively. Inspection of MRI images of these subjects exhibited the same qualitative pattern of rectus EOM size reduction as did subjects with the more common R954W substitution. After

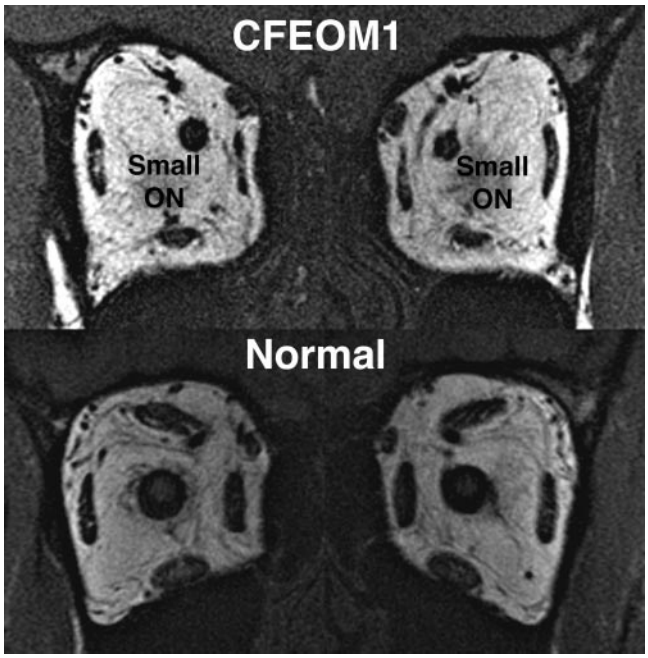

FIGURE 2. Quasicoronal MRI of orbits just posterior to the globe–ON junction illustrating a hypoplastic ON and rectus EOMs in subject 7, in comparison with a normal control subject.

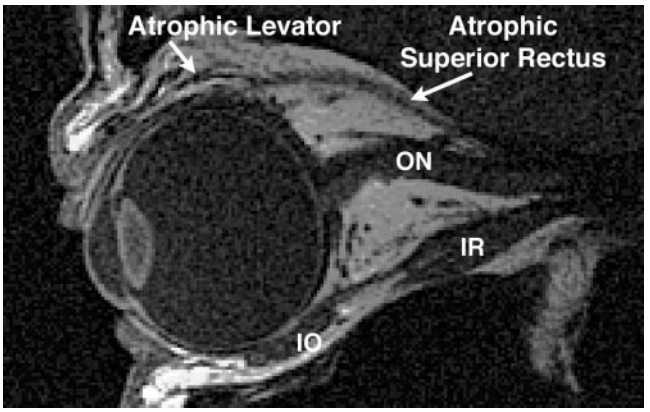

FIGURE 3. Quasisagittal MRI in subject 7 with CFEOM1 showing profound atrophy of the SR and LPS. The IR had previously undergone surgical disinsertion.

TABLE 2. Muscle Volumes in Subjects with R954W Substitution in *KIF21A*

	Control Subjects Volume (mm^3)		Subjects with CFEOM1 Volume (mm^3)	
Muscle	Mean	Standard Error	Mean	Standard Error
Medial rectus*	324	12	218	12
Superior rectus*	271	12	111	8
Lateral rectus*	328	11	282	20
Inferior rectus	277	8	240	20
Inferior oblique*	270	10	199	14

Each subject contributed data from two orbits. Volumes for rectus EOMs include contributions from six contiguous images planes extending posteriorly beginning at the globe–optic nerve junction.

* Reductions in EOM volumes of 10 subjects with CFEOM1 due to the R954W substitution were significant at 0.01 level after adjustment for multiple comparisons.

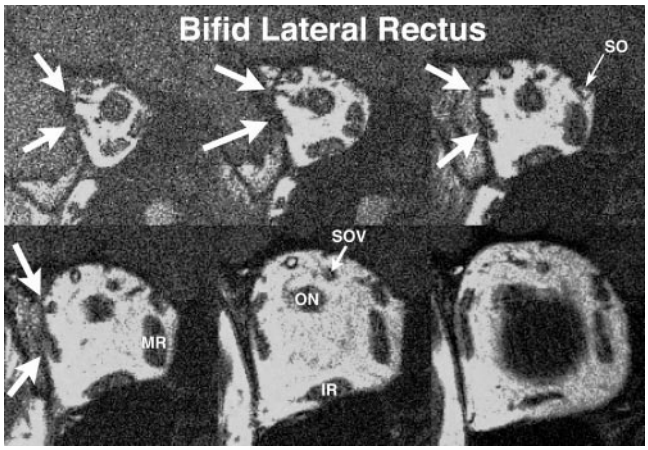

FIGURE 4. Coronal MRI of the right orbit of subject 4 with CFEOM, showing the LR muscle bifid in the deep orbit. Note the apparent absence of the SR and LPS, with preservation of the bulk of the IR and MR. Note abnormal bright signal in the SO belly.

adjustment for multiple comparisons, the only significant difference in subjects 14, 15, 17, and 19 was that the SR of subject 17 was significantly larger at 200 mm^3 ($P < 0.05$). No other EOM volumes of the subjects with rarer substitutions differed significantly from those of the AA pedigree.

Structural abnormalities of the LR muscle were found unilaterally in one and bilaterally in six subjects with the R954W amino acid substitution. Abnormalities typically consisted of a longitudinal fissure in the deep LR belly, dividing it into superior and inferior portions (Fig. 4), as well as an abnormal C-shaped configuration convex to the orbital side, and irregular internal regions of bright signal. Abnormal bright signal was also observed in multiple other EOMs, as illustrated in the MRI in Figure 5. Subject 15 with the R954Q substitution exhibited irregular internal regions of bright signal in the horizontal rectus EOMs. The origin of this abnormal bright signal is unknown, but it would not have influenced EOM size determinations because it was distinguishable from surrounding tissues. Subject 19 with the M947R substitution had bilaterally hypoplastic LR muscles. Splitting of the LR was not observed in subject 19 or 17.

Oblique EOM Size. The size of the IO was analyzed from cross sections obtained along the entire length of the EOM in quasisagittal images in 13 subjects with CFEOM1, and it was taken to be zero in subject 5, in whom the IO was bilaterally absent, and on the left in subject 10, in whom the IO was absent only on the left. The IO commonly had internal regions of abnormally bright signal and was typically hypoplastic. For subjects with the most commonly encountered R954W substitution, mean (± SD) right and left IO volumes were 164 ± 76 and 152 ± 86 mm^3, each significantly smaller ($P < 0.01$) than our previously published control values from 15 normal control IO muscles of 270 ± 38 mm^3 [21] (Table 2). The subject with the R954Q substitution exhibited small IO size bilaterally, similar to the other subjects with the R954W substitution. Subject 17 with the M356T substitution had mildly subnormal right and left IO volumes of 207 and 188 mm^3, respectively. Subject 19 with the M847R substitution had profoundly reduced right and left IO volumes of 25 and 45 mm^3, respectively.

For comparability to the published literature, SO size was assessed by maximal cross section in quasisagittal image planes. Maximum size of each SO muscle of each subject with CFEOM1 was averaged for comparison with control data, and sizes of individual SO muscles were compared with the 95% confidence limits of normal SO muscles.[22] Muscles with sizes less than the 95% confidence limit of normal were considered significantly hypoplastic. The SO was unilaterally hypoplastic in subjects 5 and 13 and bilaterally hypoplastic in subjects 4 and 10 with CFEOM1. However, over the entire group of subjects with the R954W amino acid substitution, the average maximum SO cross-sectional area of 11.4 ± 2.4 mm^2 did not differ significantly from the control size of 14.0 ± 1.3 mm^2. The average maximum SO cross-sectional area in subject 15 with the R954Q substitution was normal at 14.2 mm^2. The average maximum SO cross-sectional area in subject 17 with the M356T substitution was significantly above normal at 21.1 mm^2; the small anterior and large posterior distribution of SO volume along its length, however, suggested that this EOM in this subject had been tenotomized. Subject 19 with the M947R substitution had a significantly subnormal average maximum SO cross-sectional area of 10.4 mm^2.

Globe Position and Muscle Paths. In the first 10 subjects with CFEOM1 who were scanned and for each control subject, the globe center was computed from multiple cross sections as previously described.[19] The coordinates of the orbit center were determined from its area centroid in an image plane near the globe center. In these 10 subjects with CFEOM1, the globe center averaged 1.1 mm more nasal relative to the orbit center than in control subjects ($P < 0.01$). Linear measurements were made of the three-dimensional (3-D) location of the geometric center of each globe, comparing this with the area centroid of the bony orbit in the same MRI plane. The relationship of the vertical globe center to the orbit center did not significantly differ from normal in affected subjects. These findings were not influenced by the presence of ECO.

Paths of the rectus EOMs were determined in the preceding groups of subjects from area centroids in multiple contiguous image planes. The EOMs pass through their connective tissue pulleys, so that the anterior locations of these paths indicate the respective pulley locations in the coronal plane.[23] Because subjects with CFEOM1 were typically unable to achieve eccentric gaze positions, no inflections in rectus EOM paths were present to identify the anteroposterior coordinates of the rectus pulleys as is possible in normal subjects. It therefore was

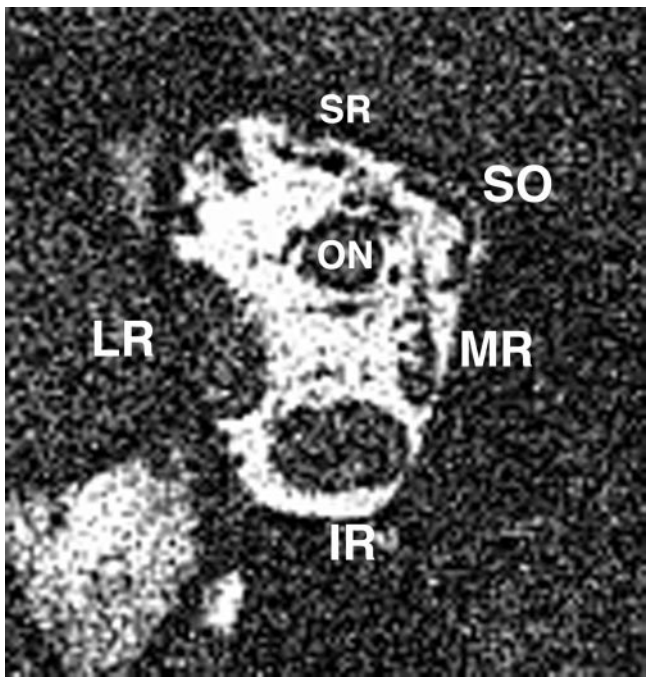

FIGURE 5. Quasicoronal MRI of the right orbit of subject 8, showing hypoplasia of the SR, SO, and MR. Note the abnormal bright signal within the MR belly. The LR and IR exhibit normal bulk.

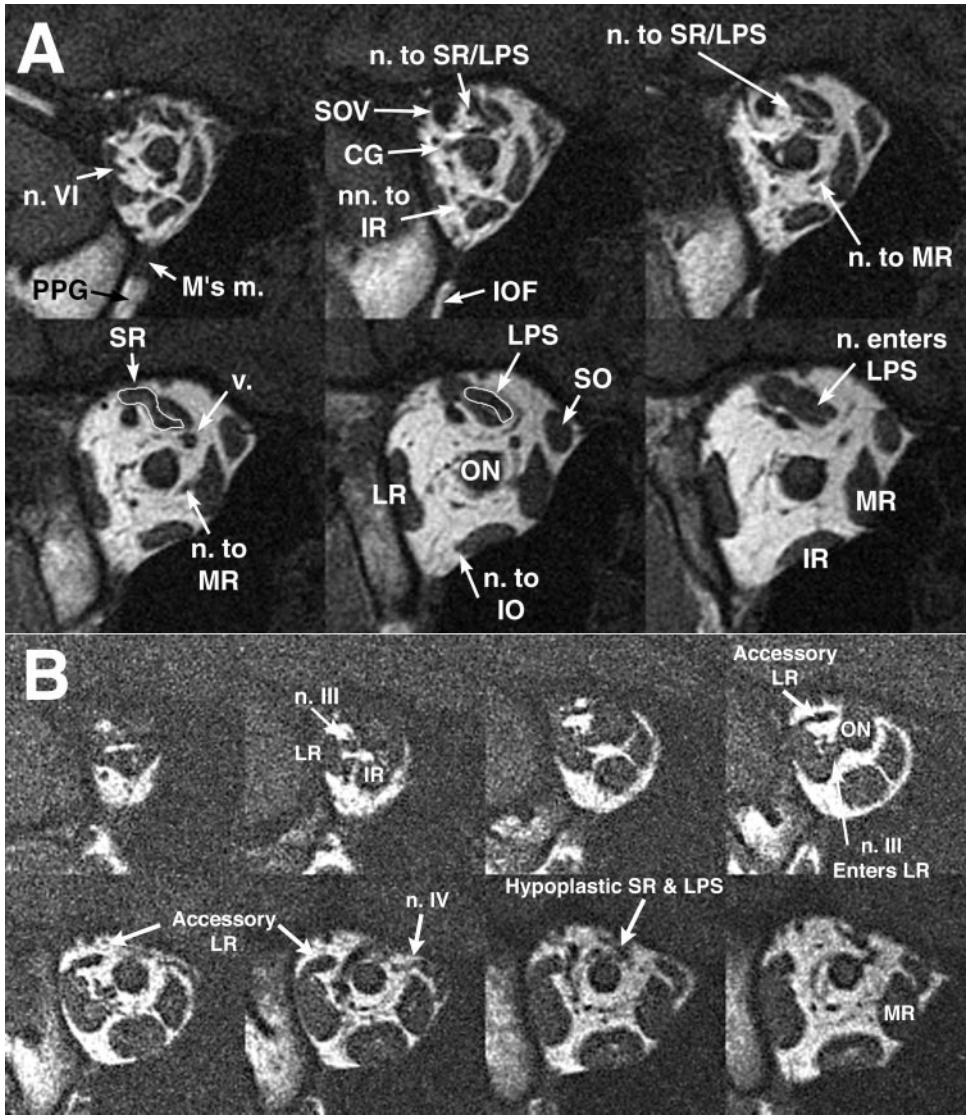

FIGURE 6. (**A**) Coronal MRI of deep right orbit of normal subject in central gaze, demonstrating details of innervation in 2-mm thickness planes. CG, ciliary ganglion; M's, Müller's muscle; PPG, pterygopalatine ganglion; SOV, superior orbital vein (v). (**B**) Coronal MRI of deep right orbit of subject 7 with CFEOM1, showing abnormal innervation. The oculomotor nerve, n. III, appears to enter mainly the LR and also the IR. The LR is divided into the main belly and an accessory LR. The SR and LPS are profoundly hypoplastic.

assumed that the anteroposterior coordinates of the rectus pulleys are the same as those known for normal subjects.[23] This was considered reasonable, since variations in anteroposterior coordinates would on geometric grounds be expected to have only a small effect on horizontal and vertical pulley coordinates. After 3-D averaging of the paths of the IR, MR, and LR in subjects with CFEOM1, the horizontal coordinates were determined at the anteroposterior locations of normal rectus pulleys. This analysis indicated that the 3-D coordinates of the MR and LR pulleys in CFEOM1 do not differ significantly from normal. The IR pulley was not in normal position in CFEOM1, being 1.6 mm more nasal and 2.6 mm more superior then normal ($P < 0.05$, after adjustment for multiple comparisons). After findings in the first 10 subjects demonstrated absence of a large effect on EOM paths, this laborious analysis was discontinued for the remaining subjects.

Imaging of Intraorbital Motor Nerves. Because the posterior orbit is less subject to motion artifacts from eye movement than is the anterior orbit, it was possible to examine in the deep orbit the motor nerves to the EOMs in image planes of 1.5- to 2-mm thickness and field of view 6 to 8 cm. In normal subjects, all the motor nerves to the EOMs could be visualized in some cases (Fig. 6A). Motor nerves to the MR, IR, IO, and LR were demonstrable in every normal case in which high-quality images were obtained, although the trochlear nerve could only occasionally be demonstrated. The inferior division of n. III can be followed from the cavernous sinus, where the n. III divides into superior and inferior divisions. By MRI, we have not been able to resolve this bifurcation in normal subjects. The superior division is small and can only occasionally be traced in normal subjects to the inferior face of the SR, where it runs anteriorly before entering the SR-LPS complex. The much larger inferior division forms a readily visualized manifold as it courses anteriorly to send out a nasal branch to the MR and an inferior branch that in turn bifurcates to innervate the IR and, more anteriorly, the IO. The motor nerve entry to the IO is compact and surrounded by the dense connective tissue of the IO pulley. The intraorbital motor nerves from the inferior division of n. III can be visualized readily and traced by MRI from the orbital apex to the target EOMs; even the epimuscular innervation of the normal LR, MR, and IR can be visualized. For these, the motor nerves typically divide to form manifolds that course anteriorly along the orbital surface of the EOMs before entering them. This is evident for the IR in the top center panel of Figure 6A. The trochlear nerve (n. IV) is small and enters the SO from a superolateral angle deep in the orbit; it was not always visualized in normal subjects. The normal abducens nerve (n. VI), which is larger than n. IV, can be seen coursing from the superior orbital apex to form a manifold along the orbital surface of the LR, where it enters to innervate it. The

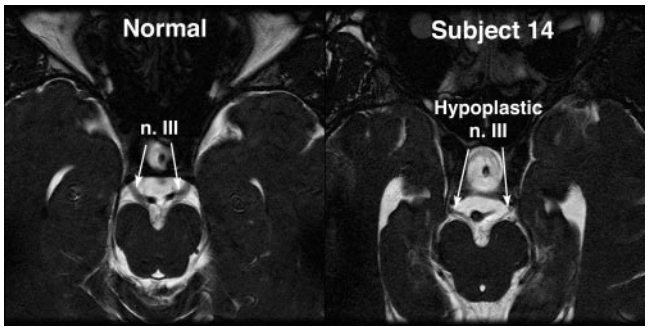

FIGURE 7. Oblique, axial heavily T2-weighted MRI images showing at *left* the normal course of the oculomotor nerve (n. III, *dark*) from the pons highlighted against the bright signal of the surrounding cerebrospinal fluid. In contrast, the nn. III of subject 14 with CFEOM1 are barely visible with the use of an identical technique.

normal n. VI and its epimuscular manifold can typically be visualized by MRI.

With knowledge of normal orbital neuroanatomy, it was possible to interpret innervation in most MRI images from subjects with CFEOM1. In addition to the structural abnormalities of EOMs, a striking and consistent feature of CFEOM1, regardless of the presence or absence of ocular motility, was abnormal motor innervation. Every demonstrable motor nerve was abnormally small in at least one orbit of each subject with CFEOM1, and most subjects with CFEOM1 had hypoplasia and/or misdirection of every motor nerve in both orbits. In no case was it possible to visualize the superior division of n. III. However, this branch cannot consistently be visualized even in normal subjects. The inferior division of n. III had size varying from apparently normal to either small or undetectable. When sufficiently large to trace, the inferior division of n. III often exhibited excessive bifurcation and appeared to enter the LR as well as its normal target EOMs. Figure 6B demonstrates coronal MRI images of the right orbit of subject 7. The deep LR was split into a main belly and an accessory band. Nearly all of the inferior division of n. III appeared to enter the LR, with only a few fine strands entering the IR and MR muscles. The suggestion of entry of the inferior division of n. III into the LR muscle was observed in MRI images in subjects 4, 7, 12, 13, 17, and 19. This finding may have been present and was not excluded in other subjects who exhibited the A pattern, because imaging quality was not adequate for tracing orbital nerves in all cases. No innervation could be identified extending to the SR and LPS in any subject with CFEOM1.

Because even normal motor nerves to individual EOMs are represented by one or at most a few pixels in the coronal image planes used in this study, the images were regarded as insufficiently precise for quantitative analysis of motor nerve size.

Imaging of Intracranial Motor Nerves. In subjects 14 and 15 with CFEOM1, and in six normal subjects, heavily T2-weighted imaging of the skull base region was conducted in 1-mm-thick slices at 390-μm resolution in a plane paralleling the optic chiasm and major cranial nerves to the orbit. This technique has just sufficient resolution to demonstrate the normal abducens nerves coursing anteriorly from the pons, but easily and consistently demonstrates the larger course of the oculomotor nerves of normal subjects (Fig. 7). Using this technique, the oculomotor nerves were strikingly small in both affected subjects (Fig. 7).

The heavily T2-weighted imaging technique demonstrated the abducens nerve in all six normal subjects (Fig. 8, left). In adjacent sections, n. VI could be traced from the pons across the cerebrospinal fluid space to the clivus in every normal subject. The n. VI was not demonstrable in any image obtained using identical technique in either of the two affected subjects, suggesting that it was too small to resolve (Fig. 8).

Findings in Affected Subjects With and Without ECO. Subjects with ECO exhibited more severe abnormalities of motor nerves and EOMs than those without ECO. The greater severity of ophthalmoplegia precluded analysis of residual motility abnormalities. Subjects with ECO exhibited two patterns on orbital imaging that were also observed in subjects without ECO. First, EOMs with principal actions reflecting the apparent angle of deviation were of substantial size, and their antagonists were hypoplastic and, in the deep orbit, exhibited an abnormal bright internal signal on T1-weighted MRI. This is illustrated in Figure 5, a deep coronal MRI in subject 8, whose globes were essentially frozen in abduction and infraduction. All of subject 8's rectus and oblique EOMs were hypoplastic, except for the LR and IR muscles, which were apparently spared. Second, there was profound hypoplasia or absence of multiple motor nerves to the EOMs. In the case of subject 8, all motor nerves were small or absent except for the abducens nerve, which appeared to innervate both the LR and IR muscles. The remaining subjects with ECO had profoundly small or absent motor nerves to all EOMs, including the abducens nerve. In most cases, the deep LR belly was split or otherwise disorganized.

Findings were generally similar in subjects without ECO, but the presence of residual motility made it possible behaviorally to confirm misinnervation of EOMs. Subjects with the R954W substitution who did not have ECO all exhibited the λ pattern of relative exodeviation in downward gaze. Multipositional MRI was informative about the mechanism of this motility pattern. In subject 7, quasicoronal plane imaging was performed of the right orbit during monocular target fixation by the left eye. During downward target fixation by the left eye, the right LR exhibited marked contractile thickening as the right eye abducted (Fig. 9). This finding suggests innervation of the LR by a motor branch of the contiguous oculomotor nerve that would normally have innervated the IR. Subject 7 also exhibited a marked superior shift of the LR path in attempted infraduction, reflecting sideslip of the LR over the globe with superior shift of its pulley (Fig. 9). Although the

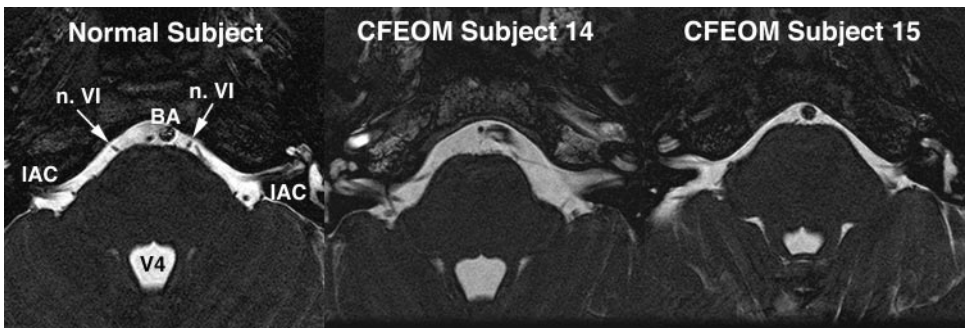

FIGURE 8. Heavily T2-weighted axial MRI images of 1-mm thickness at the level of the pons obtained in a plane paralleling the optic chiasm. In all six normal subjects, the abducens nerve (n. VI) was demonstrable. n. VI was not resolvable in either subject with CFEOM1. BA, basilar artery; IAC, internal auditory canal; V4, fourth ventricle.

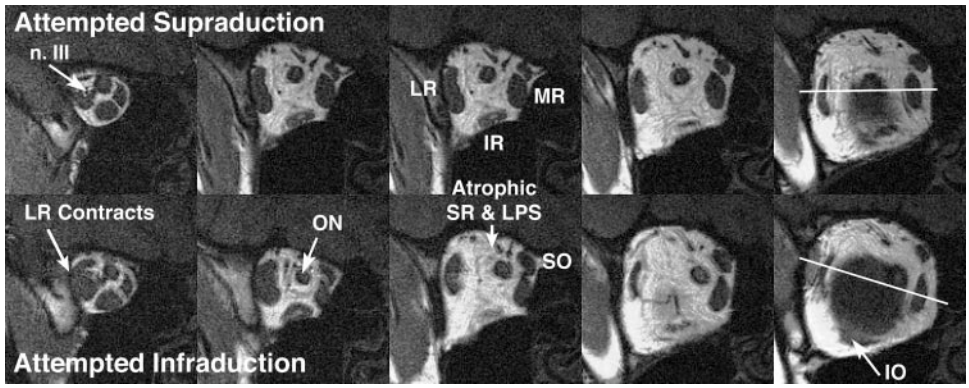

FIGURE 9. Coronal MRI of the right orbit of subject 7 with the R954W substitution, showing contractile thickening of the LR with attempted gaze shift from attempted up- to downgaze and proximity of the inferior division of the oculomotor nerve (n. III) to the LR. Globe rotation can be judged from the position of the ON at its junction with the globe (*right*); the ON is obviously hypoplastic. The noncontiguous 2-mm-thick image planes are arranged from posterior at *left* to anterior at *right*. *White lines*: centers of the LR and MR muscles, showing a superior shift of the LR in attempted downgaze.

position of the globe–ON junction in Figure 9 indicates little vertical gaze change, it confirms substantial abduction in attempted infraduction. The LR centroid, noted by the white lines in Figure 9 (right) in relationship to the MR, shifted superiorly in infraduction, reflecting sideslip over the globe despite the seeming absence of any possible contribution to this effect from the severely hypoplastic SR. The IO might have contributed to this effect by relaxation in infraduction, since IO size was normal in this case. Contractile thickening of the SO was also apparent in infraduction (Fig. 9).

Subjects 17 and 18 with the M356T substitution did not have ECO and, unlike those with the R954W substitution, did not exhibit an A or λ pattern. MRI was performed only in subject 17, who exhibited findings similar to those of the R954 substitution.

Optic Nerve. Despite the normal ophthalmoscopic appearance of the ON in all but one affected subject, the coronal plane MRI was notable for the appearance of subnormal ON size in several subjects with CFEOM1 (Fig. 2). This finding led us to perform quantitative analysis of ON cross sections from quasicoronal MRI images in affected and control subjects, and this analysis confirmed general ON hypoplasia in all except one orbit of subject 7 and one of subject 10, both of whom had the R954W substitution. Because the ON cross section normally decreases in area from anterior to posterior in the orbit due to the reduction of connective tissues surrounding the axon bundles,[24] ON cross sections were analyzed at the 2-mm image plane thickness intervals up to 10 mm posterior to the globe–ON junction in eight subjects with the R954W substitution (Fig. 10). As noted elsewhere,[24] ON cross-sectional area in the normal control group declined in a linear fashion as the ON coursed posteriorly in the orbit. This decrease of 0.387 mm^2 area/mm distance has been demonstrated to be due to reduction in connective tissue elements within the ON.[24] Subjects with CFEOM1 exhibited 30% to 40% smaller average ON cross-sectional area at every comparable location along the orbit ($P < 0.0001$), regardless of whether comparisons were based on the pooling of both eyes or on consideration of only one eye in each subject and control. In subjects with CFEOM1, the ON cross-sectional area declined at a rate of only 0.108 mm^2 area/mm distance, significantly less than in the control subjects ($P < 0.05$), so that the magnitude of difference in area of ON cross sections between the two groups diminished modestly in the posterior orbit. There was no clear correlation between ON cross-sectional area and visual acuity in subjects with CFEOM.

DISCUSSION

The clinical findings of blepharoptosis and strabismus are not highly specific, rendering them susceptible to phenocopy from a wide variety of causes, as well as to potential variation in presentation. In this study, we used high-resolution MRI to investigate the internal phenotype, or endophenotype, of a well-defined, homogeneous group of subjects with CFEOM1 resulting from mutations in *KIF21A*. The endophenotype that emerged is remarkably uniform, regardless of the specific *KIF21A* mutation and is largely consistent with the clinical findings and the previous neuroanatomic study of CFEOM1.

Confirmation and Extension of Existing Data

All subjects with CFEOM1 due to *KIF21A* mutations exhibited clinical findings of blepharoptosis and limited supraduction. These clinical findings correlated in all subjects with profound hypoplasia of the LPS and SR muscles, both of which are innervated by the superior division of n. III. This finding is consistent with the existing autopsy evidence of abnormalities of the superior division of n. III in CFEOM.[1] The current findings of a small nn. III exiting the brain stem supports the autopsy findings of a quantitative decrease in number of axons and overall size in the proximal common trunk of n. III.[1] Of course, severe decrease in the number of axons may render n. III branches too small to detect at all using MRI, as was found in the current study for some subjects with CFEOM1.

Many EOMs in CFEOM were found by MRI to be hypoplastic, to have grossly abnormal morphology, or to have abnormal internal signal characteristics. This confirms and extends the

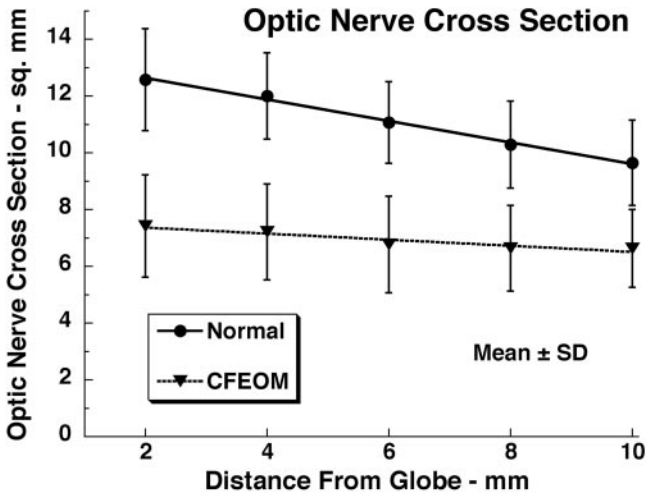

FIGURE 10. Cross-sectional area of optic nerve in CFEOM1 and normal subjects. Data average both orbits of each subject, but the significant differences between groups persisted with analysis of either the right or left eye individually. Linear fits to the data in both groups yielded negative slopes that differed ($P < 0.05$).

autopsy finding of internal abnormalities in EOMs innervated both by n. III and other cranial nerves. The abnormal MRI signals so commonly observed in this study may correspond to the mitochondrial aggregates observed in histologic study of EOMs obtained at autopsy.[1]

The present findings confirm widespread misinnervation of EOMs in CFEOM1. Particularly common was A-pattern strabismus, with relative exodeviation in attempted downward gaze. MRI confirmed that this is due to LR contraction in downward gaze, presumably because the LR is innervated by a branch of n. III normally destined to innervate the IR muscle.

New Structural Findings in CFEOM

Severe generalized ophthalmoplegia was also common in these subjects with CFEOM1 and correlated with the novel but variable MRI finding of hypoplastic or absent motor nerves to all the EOMs. This would not have been anticipated, because innervation was present in other EOMs at autopsy.[1] Abnormalities were frequently found in the inferior division of n. III, as well as n. VI at its exit from the brain stem and in the orbit. Although even a normal n. IV cannot be resolved reliably by MRI, the frequent finding of SO hypoplasia suggests that n. IV is also involved. Nevertheless, preservation of SO volume in most cases of CFEOM1 suggests that n. IV is at least relatively spared, or else more capable of terminal sprouting than n. III.

The n. VI was hypoplastic in the orbit in many cases of CFEOM1, and in the skull base in both cases imaged. This is a surprising finding in light of the presence of the nerve in one autopsy case.[1] Presumably, n. VI is relatively less affected than n. III in CFEOM1, or perhaps, when hypoplastic, n. VI is more capable of terminal sprouting to maintain LR muscle bulk.

The present study provides suggestive imaging evidence for innervation of the LR muscle by a branch of n. III. This evidence includes contractile thickening of LR on attempted downward gaze. Although MRI resolution is inadequate to confirm the presence of motor endplates in the LR, the inferior division of n. III is consistently seen to run adjacent to the deep portion of the LR where n. VI normally enters and arborizes. It is thus very plausible that the LR is innervated by n. III in CFEOM1. In CFEOM1 the deep LR was commonly split or otherwise structurally disorganized. We propose that normal n. VI innervation is essential for normal structure of the deep LR belly. The uniformly profound hypoplasia of SR and LPS in CFEOM1 argues that the superior division of n. III is congenitally absent. We propose that variability in the severity and pattern of ophthalmoplegia in CFEOM1 depends on the degree to which residual axons of the hypoplastic inferior division of n. III reach their normal target EOMs or are misdirected to innervate the LR. Both n. IV and VI are affected to variable degrees in CFEOM1, although there is currently little evidence that they are misrouted to inappropriate EOMs. There was a suggestion of misrouting of n. VI to IR in subject 8. Misrouting of n. III in CFEOM1 is more likely the result of anatomic proximity than of inherent promiscuity of the nerve. It is probable that n. III is commonly misrouted to LR because n. III's normal path takes it adjacent to the LR's nerve entry site. No similar proximity of n. IV or VI occurs in other EOMs.

ON Involvement in CFEOM

Quantitative MRI has recently emerged as a powerful technique for ON analysis.[24] Subjects with CFEOM1 due to *KIF21A* mutations consistently exhibited the novel yet subclinical finding of approximately 30% to 40% reduction in ON cross-sectional area. Although KIF21A is expressed within many neuronal populations in the mature mouse brain, including the mouse retina,[14] the reported human *KIF21A* phenotype has been limited to ptosis and defects in ocular motility. Our additional observation of ON hypoplasia suggests that KIF21A also plays a role in the development or maintenance of the ON and that this role is disrupted by these specific *KIF21A* mutations.

Although the ON hypoplasia was statistically significant, it was severe enough to be evident at ophthalmoscopy in only one subject, highlighting the insensitivity of clinical evaluation of ON size. None of the subjects with CFEOM1 had gross visual field deficits or afferent pupillary defects. In addition, although ON hypoplasia may contribute to visual disability in CFEOM1,[24] there was no severe visual loss attributable to ON hypoplasia in the current subjects with CFEOM1. More common causes of visual loss probably included amblyopia and corneal scarring due to exposure keratopathy. Subjects with CFEOM1 had significantly subnormal pupil diameters. This may be related to an efferent cause such as n. III or oculosympathetic abnormality, but does not have an obvious relationship to ON hypoplasia.

Absence of Widespread Pulley Abnormalities

Pulley disorders are now recognized as causes of strabismus.[16,25] Marked abnormalities of rectus EOM paths due to misplaced pulleys are commonly associated with craniosynostosis syndromes and are caused by mutations in *FGFR*,[26] in which orbital nerves and EOM volumes are presumably otherwise normal. This contrasts with CFEOM1, in which EOM paths are normal or only minimally abnormal (as for the IR). Profound ophthalmoplegia in subjects with CFEOM1 precluded detection of the inflections in EOM paths in secondary gaze positions that define anteroposterior pulley locations, which we assumed to be normal. Even if subtly abnormal, however, anteroposterior malpositioning of rectus pulleys has not been reported to be associated with severe incomitant strabismus such as the typical A pattern observed in this study in CFEOM1. The present finding of a 1.1-mm nasal shift in the position of the globe center in CFEOM1 is probably due to a combination of EOM hypoplasia and the temporal angulation of the long axes of the two orbits. Widespread EOM hypoplasia would reduce the soft tissue volume of the bony orbits, allowing the globes to shift posteriorly and nasally along the long axes of the orbits without much effect on EOM pulling directions. These considerations notwithstanding, the positions of the rectus pulleys in the coronal plane remained remarkably normal in CFEOM1. It may be concluded that normal EOM innervation is not necessary for establishment and maintenance of normal rectus pulley positions. This is further evidence that pulley abnormalities are primary in cases of incomitant strabismus with which they are associated[27–29] and that pulley heterotopy is unlikely to be secondary to acquired EOM denervation.[28] Pulley disease may instead arise from mutations affecting the neural crest progenitors of the pulleys, or from factors affecting the bony or soft tissue constituents of the pulley supports. Cocontraction of antagonist EOMs was associated with gaze-dependent orbital pulley shift[30] in subject 7, analogous to LR sideslip due to cocontraction in Duane syndrome.[31]

Cause of ECO Versus Residual Movement

Some subjects with CFEOM1 exhibited ECO, whereas others, including affected members of the same family harboring the same mutation, had greater preservation of ocular motility. This suggests that ECO is not a qualitative feature of CFEOM1, but merely the extreme end of a spectrum of severity of gene expression that may be modified by environment and/or genetic background. Even in ECO, fine nystagmus and preservation of low-amplitude convergence were typically observed. This suggests sparing of some residual innervation and residual

EOM fibers, even in EOMs severely affected by CFEOM. The only oculorotary EOM with no activity at all in CFEOM1 was the SR. At the other end of the spectrum, EOMs that would have been regarded as clinically normal in relatively mild cases of CFEOM1 typically had hypoplastic motor innervation. This finding reinforces the value of imaging to determine the endophenotype in ocular motility disorders.

Comparisons of both the clinical and MR imaging results among and between individuals with each of the four *KIF21A* mutations did not yield any clearly distinguishing features that could be used to predict specific mutations among patients with CFEOM1. The generalized hypoplasia of the orbital motor and ONs, as well as the frequent finding of aberrant innervation of EOMs, continue to support a primary neural pathology underlying CFEOM1 and a role for *KIF21A* in the development of these neural circuits.

References

1. Engle EC, Goumnerov BC, McKeown CA, et al. Oculomotor nerve and muscle abnormalities in congenital fibrosis of the extraocular muscles. *Ann Neurol*. 1997;41:314–325.
2. Engle EC, Kunkel LM, Specht LA, Beggs AH. Mapping a gene for congenital fibrosis of the extraocular muscles to the centromeric region of chromosome 12. *Nat Genet*. 1994;7:69–73.
3. Engle EC, Marondel I, Houtman WA, et al. Congenital fibrosis of the extraocular muscles (autosomal dominant congenital external ophthalmoplegia): genetic homogeneity, linkage refinement, and physical mapping on chromosome 12. *Am J Hum Genet*. 1995; 58:1086–1094.
4. Yamada K, Andrews C, Chan W-M, et al. Heterozygous mutations of the kinesin KIF21A in congenital fibrosis of the extraocular muscles type 1 (CFEOM1). *Nat Genet*. 2003;35:318–321.
5. Brown HW. Congenital structural muscle anomalies. In: Allen JH, ed. *Strabismus Ophthalmic Symposium.* St. Louis: CV Mosby; 1950:205–236.
6. Crawford JS. Congenital fibrosis syndrome. *Can J Ophthalmol*. 1970;5:331–336.
7. Harley RD, Rodrigues MM, Crawford JS. Congenital fibrosis of the extraocular muscles. *Trans Am Ophthalmol Soc*. 1978;76:197–226.
8. Laughlin RC. Congenital fibrosis of the extraocular muscles: a report of six cases. *Am J Ophthalmol*. 1956;41:432–438.
9. Apt L, Axelrod N. Generalized fibrosis of the extraocular muscles. *Am J Ophthalmol*. 1978;85:822–829.
10. Brodsky MC, Pollock SC, Buckley EG. Neural misdirection in congenital ocular fibrosis syndrome: Implications and pathogenesis. *J Pediatr Ophthalmol Strabismus*. 1989;26:159–161.
11. Cibis GW, Kies R, Lawwill T, Varghese G. Electromyography in congenital familial ophthalmoplegia. In: Reinecke RD, ed. *Strabismus II.* New York: Grune & Stratton; 1984:379–390.
12. Houtman WA, van Weerden TW, Robinson PH, de Vries B, Hoogenraad TU. Hereditary congenital external ophthalmoplegia. *Ophthalmologica*. 1986;193:207–218.
13. Brodsky MC. Hereditary external ophthalmoplegia, synergistic divergence, jaw winking, and oculocutaneous hypopigmentation. *Ophthalmology*. 1998;105:717–725.
14. Marszalek JR, Weiner JA, Farlow SJ, Chun J, Goldstein LS. Novel dendritic kinesin sorting identified by different process targeting of two related kinesins: KIF21A and KIF21B. *J Cell Biol*. 1999;145: 469–479.
15. Ginkel LM, Wordeman L. Expression and partial characterization of kinesin-related proteins in differentiating and adult skeletal muscle. *Mol Biol Cell*. 2000;11:4143–4158.
16. Demer JL. A 12 year, prospective study of extraocular muscle imaging in complex strabismus. *J AAPOS*. 2003;6:337–347.
17. Seitz J, Held P, Strotzer M, et al. MR imaging of cranial nerve lesions using six different high-resolution T1 and T2(*)-weighted 3D and 2D sequences. *Acta Radiol*. 2002;43:349–353.
18. Demer JL, Miller JM. Orbital imaging in strabismus surgery. In: Rosenbaum AL, Santiago AP, eds. *Clinical Strabismus Management: Principles and Techniques.* Philadelphia: WB Saunders; 1999:84–98.
19. Clark RA, Miller JM, Demer JL. Three-dimensional location of human rectus pulleys by path inflections in secondary gaze positions. *Invest Ophthalmol Vis Sci*. 2000;41:3787–3797.
20. Kono R, Clark RA, Demer JL. Active pulleys: magnetic resonance imaging of rectus muscle paths in tertiary gazes. *Invest Ophthalmol Vis Sci*. 2002;43:2179–2188.
21. Demer JL, Oh SY, Clark RA, Poukens V. Evidence for a pulley of the inferior oblique muscle. *Invest Ophthalmol Vis Sci*. 2003;44: 3856–3865.
22. Kono R, Demer JL. Magnetic resonance imaging of the functional anatomy of the inferior oblique muscle in superior oblique palsy. *Ophthalmology*. 2003;110:1219–1229.
23. Clark RA, Miller JM, Demer JL. Location and stability of rectus muscle pulleys inferred from muscle paths. *Invest Ophthalmol Vis Sci*. 1997;38:227–240.
24. Karim S, Clark RA, Poukens V, Demer JL. Quantitative magnetic resonance imaging and histology demonstrates systematic variation in human intraorbital optic nerve size. *Invest Ophthalmol Vis Sci*. 2004;45:1047–1051.
25. Oh SY, Clark RA, Velez F, Rosenbaum AL, Demer JL. Incomitant strabismus associated with instability of rectus pulleys. *Invest Ophthalmol Vis Sci*. 2002;43:2169–2178.
26. Muller U, Steinberger D, Kunze S. Molecular genetics of craniosynostotic syndromes. *Graefes Arch Clin Exp Ophthalmol*. 1997; 235:545–550.
27. Clark RA, Miller JM, Rosenbaum AL, Demer JL. Heterotopic muscle pulleys or oblique muscle dysfunction? *J AAPOS*. 1998;2:17–25.
28. Clark RA, Miller JM, Demer JL. Displacement of the medial rectus pulley in superior oblique palsy. *Invest Ophthalmol Vis Sci*. 1998; 39:207–212.
29. Demer JL, Clark RA, Miller JM. Heterotopy of extraocular muscle pulleys causes incomitant strabismus. In: Lennerstrand G, ed. *Advances in Strabismology.* Buren, The Netherlands: Aeolus Press; 1999:91–94.
30. Demer JL, Kono R, Wright W, Oh SY, Clark RA. Gaze-related orbital pulley shift: a novel cause of incomitant strabismus. In: de Faber JT, ed. *Progress in Strabismology.* Lisse, The Netherlands: Swets and Zeitlinger; 2002:207–210.
31. Miller JM, Demer JL, Rosenbaum AL. Two mechanisms of upshoots and down-shoots in Duane's syndrome revealed by a new magnetic resonance imaging (MRI) technique. In: Campos EC, ed. *Strabismus and Ocular Motility Disorders.* London: Macmillian Press; 1990:229–234.